Case Studies in Construction Materials 12 (2020) e00328

Contents lists available at ScienceDirect

Case Studies in Construction Materials

journal homepage: www.elsevier.com/locate/cscm

Case study

# Effect of partial replacement of coarse aggregate by polystyrene balls on the shear behaviour of deep beams with web openings

Ibrahim G. Shaaban[a,*], Amr H. Zaher[b], Mohamed Said[c], Wael Montaser[d], Mohamed Ramadan[d], Ghada N. Abd Elhameed[d]

[a] Civil Engineering and Built Environment, University of West London, UK
[b] Structural Eng. Dept., Faculty of Eng., Ain Shams University, Cairo, Egypt
[c] Civil Engineering Department, Faculty of Engineering, Shoubra, Benha University, Egypt
[d] Structural Eng. Dept., Faculty of Eng., October 6 University, Giza, Egypt

ARTICLE INFO

*Article history:*
Received 11 September 2019
Received in revised form 6 December 2019
Accepted 16 December 2019

*Keywords:*
Coarse aggregate
Polystyrene balls
Deep beams
Shear strength
Web openings
Finite element model
Strut-and-Tie model

ABSTRACT

Thirteen specimens were experimentally tested under single midspan concentrated loads to study the shear behavior of lightweight concrete (LWC) and normal weight concrete (NWC) deep beams with web openings. In this research, the term LWC refers to the concrete obtained by partially replacing aggregate by polystyrene foam balls not the concrete containing lightweight aggregate. This resulted in a weight reduction of LWC beams in this research by approximately 30% compared to NWC compartments. The studied variables were the dimensions and location of openings, transverse reinforcement ratio, and shear span to depth ratio (a/d). It was found that the overall shear behavior and failure mode for LWC deep beams are comparable to those of the NWC specimens. This is very promising and encouraging to build lighter deep beams of similar structural behaviour as that of NWC deep beams. Dimensions of the openings have a significant effect on the behaviour of failure and shear strength of LWC and NWC deep beams. It was found that increasing the depth of the opening from 20 % to 40 % of the beam depth led to a reduction in the ultimate load by up to 46.4 %. Finite element modelling of the test beams was carried out to verify numerical results versus experimental work and both were very well correlated. In addition, a parametric study was conducted to assess the effect of internal stiffening around openings in deep beams. The maximum enhancement in the shear capacity was approximately 30 % for beams, internally strengthened by additional reinforcement on the perimeter of openings compared to the beams without any reinforcement around the openings. Strut-and-Tie model (STM) was carried out as a rational approach to predict the shear behaviour of studied beams. It was found that STM underestimates the shear of the studied beams compared to experimental results for different tested beams but the agreement between both of them was acceptable. It is recommended that the depth of opening should not exceed 20 % of the depth of the deep beam and if the depth of opening is more than that or lies in the shear span it is highly recommended to strengthen the opening internally by additional reinforcement around its perimeter.


* Corresponding author.
*E-mail address:* ibrahim.shaaban@uwl.ac.uk (I.G. Shaaban).

https://doi.org/10.1016/j.cscm.2019.e00328

**Nomenclature**

| | |
|---|---|
| *Sh* | Spacing between horizontal web reinforcement |
| *Sy* | Spacing between vertical web reinforcement |
| *dv* | Diameter of vertical stirrups |
| $\rho v$ | Transverse reinforcement ratios |
| *Av* | The area of a vertical stirrup within a distance |
| w/c | Water cement ratio |
| *F* | A function of the principal stress state; $\sigma xp$,$\sigma yp$, $\sigma zp$ |
| *S* | Failure surface expressed in terms of principal stresses and the strength parameters ft, fc, $f_cb$, $f_1$ and $f_2$ |
| $f_t$ | Ultimate uniaxial tensile strength |
| $f_c$ | Ultimate uniaxial compressive strength |
| $f_{cc}$ | Concrete peak stress |
| $f_{cb}$ | Ultimate biaxial compressive strength |
| $f_1$ | Ultimate compressive strength for a state of biaxial compression superimposed on hydrostatic stress state |
| $f_2$ | Ultimate compressive strength for a state of uniaxial compression superimposed on hydrostatic stress state |
| $f_{cu}$ | Cube compressive strength of concrete |
| $f_c'$ | Cylinder compressive strength |
| *a/d* | Shear span-to-depth ratio |
| $f_s$ and $\varepsilon_s$ | The average stress and strain of steel bars, respectively |
| $f_y$ *and* $\varepsilon_y$ | The yield stress and strain of steel bars, respectively |
| *Es* | The young's modulus of steel reinforcement |
| $f_{cr}$ | The cracking strength of concrete |
| $\varepsilon_c$ | Concrete strain |
| $\varepsilon_{c1}$ | Concrete strain at ultimate stress |
| $\varepsilon_{cc1}$ | Concrete strain at peak stress |
| $\varepsilon_n$ | Strain in steel bars |
| *FEM* | Finite element method |
| *h* | The beam height |
| *d* | The beam depth |
| *b* | The beam width |
| *a* | The shear span |
| *a1* | The height of node N1 |
| *a2* | The height of node N2 |
| *b1* | The length of bearing plate 1 |
| *b2* | The length of bearing plate 2 |
| *Ld* | The internal lever arm between the tie force T, and compression strut S2 |
| *S* | The force in strut S |
| *N1* | The node N1 |
| *N2* | The node N2 |
| *W11* | The width of strut S at node N1, measured perpendicular to strut center line |
| *W12* | The width of strut S at node N2, measured perpendicular to strut center line |
| *W1av* | The average width of strut W11 and W12; |
| *L* | The beam effective length |
| $\alpha$ | The inclination of strut S |
| *C* | The concrete cover |
| $\Phi_{str}$ | The stirrup diameter |

| | |
|---|---|
| $\varphi_i$ | The longitudinal steel diameter |
| $n$ | The number of steel layers |
| $s$ | The spacing between steel layers |
| $As$ | The area of the reinforcement |
| $V$ | The shear force at support |
| $f^{s}ce$ | The effective concrete compressive strength for strut S |
| $f^{N1}ce$ | Effective concrete compressive strength at node N1 |
| $f^{N2}ce$ | Effective concrete compressive strength at node N2 |

## 1. Introduction

Deep beams are used in special structures such as transfer floors of high-rise buildings, offshore structures and complex foundation systems. The shear capacity is the governing design factor for deep beams. In simple deep beams, the zone of high shear coincides with the district of low moment. Different values of the span to depth ratio ($L_e$/d) and the shear span to depth ratio (a/d) are proposed by different design codes to define deep beams [35,40]. Openings in the web area are often provided for critical services and accessibility. The ventilating slots are the ideal example for the opening in deep beams. Such openings may affect the capacity or the stresses distribution, particularly when openings exist in the critical regions. The shear capacity of beams with openings is based on numerous factors, such as: location, dimensions of the opening, and properties of used materials (e.g. concrete and steel) [1,2]. Simplified design methods for deep beams without special consideration to the influence of web openings are described in most of the available international design codes [35,40].

Extensive analytical, numerical, and experimental investigations have been carried out for studying deep beams with web openings [3–11]. Mansur and Alwist [12] experimentally tested 12 reinforced fiber concrete deep beams (1300 × 650 mm) with small size openings (175 × 125 mm). Their results indicated that the amount of web reinforcement (fibers or continuous steel reinforcement), and the location of opening are the principal parameters that affect the strength of deep beams. They predicted the strength using equations for non-fiber concrete deep beams with reasonable accuracy. Shanmugam and Swaddiwudhipong [13] developed an empirical formula to predict the ultimate strength of experimentally tested fiber reinforced concrete deep beams containing openings. Their results showed that the ultimate strength primarily depends upon the extent to which the opening intercepts the natural load path. Ashour [14] developed a model for a mechanism of shear failure of analyzed specimens. The model presented that a/d ratio has a higher influence on the shear capacity than that of the $L_e$/d ratio.

Sahoo et al. [15] investigated the performance of two RC and two steel fiber-reinforced concrete (SFRC) deep beams with large openings under monotonically increased concentrated loads. The boundary regions near the supports of two studied specimens were strengthened with steel cages formed by steel reinforcement bars. They found that the RC specimen with strengthened boundaries exhibited a ductile mode of failure and had significantly higher ultimate strength than that predicted by Strut and Tie Models (STMs). They found also that the SFRC specimens with 1.5 % volume fraction of fibers reached much higher strength than the design load and exhibited significant postpeak residual strength and a ductile mode of failure. Doh et al. [16] carried out a parametric study for high strength concrete deep beams with various web openings configurations using nonlinear-layered finite element method (LFEM). Their results confirmed that the current design methods are inadequate in predicting the maximum shear strength when web openings are present.

Abduljalil [17] carried out an experimental work to study shear resistance of reinforced concrete deep beams with opening strengthened by CFRP strips. He found that externally CFRP strips significantly increased the ultimate shear capacity and they limited the shear crack width of the deep beams with openings. Adam et al. [18] carried out experimental and finite element study for self-compacted concrete solid deep beams with fibers. They found that both vertical and horizontal web reinforcement are efficient in shear capacity enhancement of studied specimens. They also found that ultimate shear capacity was increased by about 47 % with increasing the longitudinal steel ratio from 1.0% to 2.2%. Hussain [19] developed a finite element model using ANSYS software release 12.0 program to study the ultimate load and crack propagation for reinforced NSC specimens provided with openings. His results presented acceptable agreement with experimental results of ultimate beam capacity, corresponding mid span deflection, and detected inclined cracks.

The use of LWC structures, especially deep beams, is increasing widely. These beams are efficient since their ultimate strength can be comparable to NWC counterparts at an approximate weight of only sixty percent of that for NWC deep beams. Huang et al. [20] studied experimental shear behavior of full dimension LWC solid deep beam specimens. Their results concluded that the failure modes of LWC beams are similar to those of NWC beams, including shear-compression failure and shear-tension failure. Sathiyamoorthy [21] found that shear strength of LWC beams increased with the decrease of a/d ratio. He reported that LWC beams showed higher number of cracks and wider crack width at failure compared to their NWC counterparts. He also mentioned that the international design building codes [35,40] are conservative in predicting shear strength of shear/non-shear reinforced LWC beams. Back in 1973, Kong and Sharp [22] studied the shear strength of

**Table 1**
Experimental program.

| Concrete type | Group | Beam | Shear span to depth ratio (a/d) | Stirrups | | | Opening* Notation |
|---|---|---|---|---|---|---|---|
| | | | | $S_h$ (mm) | dv (mm) | ρv =Av /$s_v$ b (%) | |
| LWC | 1 | $B_{LWC1}$ | 0.97 | 100 | 6 | 0.707 | – |
| | | $B_{LWC2}$ | 0.97 | 100 | 6 | 0.707 | 1A13 |
| | | $B_{LWC3}$ | 0.97 | 100 | 6 | 0.707 | 1A12 |
| | | $B_{LWC4}$ | 0.97 | 100 | 6 | 0.707 | 2A12 |
| | 2 | $B_{LWC5}$ | 0.97 | 160 | 6 | 0.442 | 1B22 |
| | | $B_{LWC6}$ | 0.97 | 160 | 6 | 0.442 | 2B22 |
| | | $B_{LWC7}$ | 0.97 | 160 | 6 | 0.442 | 2B21 |
| | | $B_{LWC8}$ | 1.63 | 160 | 6 | 0.442 | 1B22 |
| | | $B_{LWC9}$ | 2.08 | 160 | 6 | 0.442 | 1B22 |
| NWC | 3 | $B_{NWC6}$ | 0.97 | 160 | 6 | 0.442 | 2B22 |
| | | $B_{NWC7}$ | 0.97 | 160 | 6 | 0.442 | 2B21 |
| | | $B_{NWC8}$ | 1.63 | 160 | 6 | 0.442 | 1B22 |
| | | $B_{NWC9}$ | 2.08 | 160 | 6 | 0.442 | 1B22 |

*Opening notations are shown in Fig. 2.

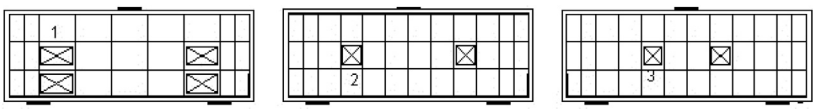

Location of openings & Opening Notation

LWC deep beams with small size of their openings and they developed a semi-empirical method for the analysis of deep beams with small openings. It is worth mentioning that LWC deep beams studied in literature and mentioned above are those containing light weight aggregates.

It can be seen from the review above that further research is needed for accurate prediction of strength and behaviour of LWC deep beams cast by partially replacing coarse aggregates by polystyrene foam balls with openings of large dimensions. The authors of the current investigation started a project in 2015, funded by two Egyptian universities, namely: Ain Shams and October 6, to study the LWC deep beams containing polystyrene balls with openings [23,24]. The current study investigates the effect of opening size, location and number of openings on the shear behavior of both LWC and NWC deep beams subjected to concentrated loads. Other studied variables include the transverse reinforcement ratio and a/d ratio. Experimental work is carried out and theoretical work included prediction of experimental results using the rational method, Strut-and-Tie Model (STM), and the more accurate one, three-dimensional Finite Element Modeling (FEM). STM approach follows Foster and Lan Gilbert [25] while FEM is developed using ANSYS package (ANSYS 13.0) to predict the results and to evaluate its sensitivity to the studied parameters. In addition, a parametric study is carried out to further study the effect of increasing the longitudinal main reinforcement ratio, the internal stiffening of the opening perimeter using additional reinforcement on the shear behavior of LWC deep beams with openings. Ultimately, recommendations are introduced for the analysis and design of LWC deep beams with openings.

## 2. Experimental program

### *2.1. Preparation of test specimens*

The program includes thirteen LWC and NWC deep beams. Beams were tested under a single midspan concentrated load. Deformed steel, grade 40/60 were used for longitudinal top and bottom reinforcement. The bottom bars consisted of four deformed bars of 16 mm diameter in two layers while the top reinforcement consisted of two bars of 10 mm diameter. The specimens were designed to ensure that shear failure occurs. Adequate anchorage was provided to the longitudinal bars. Mild steel, grade 24/35, of 6-mm and 8-mm diameter was used as horizontal and vertical shear reinforcement. Additional precautions were taken at the supports by placing bearing plates (100 × 100 × 15 mm) under the load position in order to prevent local failure by bearing. Specimens were divided into three groups as indicated in Table 1. All the tested specimens had the same rectangular cross-section of 80 mm width and 400 mm total height as shown in Figs. 1–2. Mix design, of both of NWC and LWC, was carried out to achieve similar target cube strength after 28 days. Light weight concrete (LWC) were made by partially replacing coarse aggregate by polystyrene foam balls. This resulted in a reduction of overall weight of the LWC test beams by approximately 30 % compared to their counterparts of NWC ones. Table 2 displays the mix design for LWC and NWC. Mechanical properties of LWC and NWC mixes are recorded in Table 3.

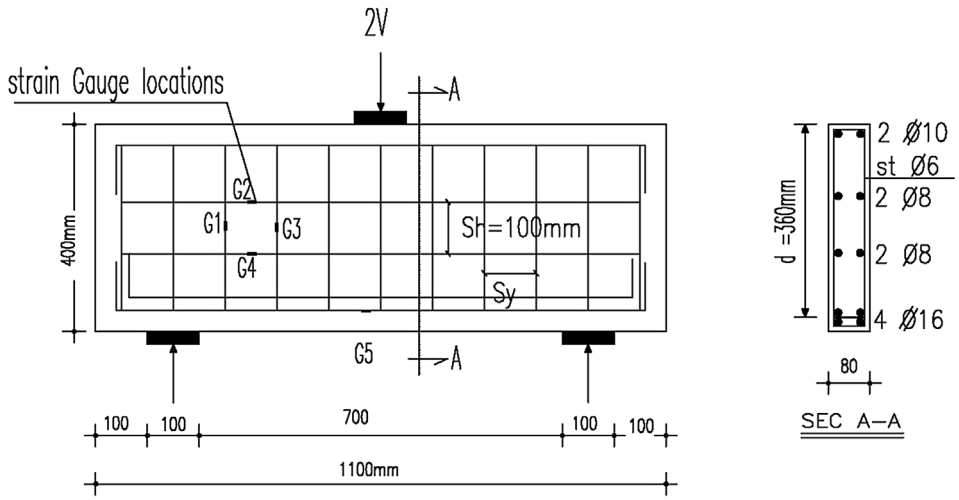


**Fig. 1.** Reinforcement details.

### 2.2. Description of test specimens

Table 1 and Fig. 2 show that the openings arrangements were either single row of openings, having a height equals to 20 % of the beam total height; or double rows of openings having a height equals to 40 % of the beam total height. Three different locations of the openings were tested; location 1, 2 and 3. For location 1, the opening lies between the first stirrup at the support and the second one. For location 2, the opening lies between the second stirrup from the support and the third one. Regarding location 3, the opening lies between the third stirrup from the support and the fourth one. The locations of web openings were selected to test three different load flows to the support. Spacing ($S_v$) between the vertical web reinforcement was 100 mm and 200 mm. Three different values of a/d ratio; 0.97, 1.63 and 2.08, were considered. The beam notation, as indicated in Table 1, included four parts. The first part refers to the number of openings in the shear span (1 or 2) and the second part indicated the size of opening (A = width x height = 80 $\times$ 80 mm and B = 140 $\times$ 80 mm). The third part referred to the web reinforcement arrangement (1 for $S_v$ = 100 mm and 2 for $S_v$ = 200 mm) and the fourth part referred to the position of the openings (location 1, 2 and 3).

### 2.3. Loading and test procedure

Specimens were loaded in increments up to failure. Specimens were instrumented to measure their deformational behavior. The recorded data include measurements of strain in concrete, main steel, transverse reinforcement (stirrups) and longitudinal bars strain; deflection and crack propagation. The strain gauge was shown in Fig. 1. The deflections were recorded using three LVDT, Fig. 3. LVDT were arranged to measure the deflection distribution. The cracks were traced at each increment.

## 3. Experimental results and discussion

Crack pattern and failure modes, deflections, and steel strains for horizontal, vertical stirrups and main bars reinforcement were noted for each of the thirteen specimens and the relationships are plotted in Figs. 4–11. The ultimate loads and deflections are recorded, Table 4.

### 3.1. Crack pattern and failure modes

Fig. 4 displays the crack patterns which were in terms of flexural and shear cracking for all the test specimens. For all specimens, the flexural crack was initiated at the central of the beam span. Flexural cracks were distributed as the load increased. For solid beam $B_{LWC1}$, the tensile cracks initiated on the tension side of the beam span. The cracks propagated upward with the increase of loading. Diagonal cracks suddenly developed at the shear span. The cracks were detected parallel to the compression strut. The cracks were spread towards the loading region and supports. A typical shear compression failure of beam $B_{LWC1}$ occurred suddenly by crushing in the concrete compression struts resulting also in a loud noise. Finally, sudden shear failure occurred instantly after main diagonal cracks formed within one or two side of the shear span as shown in Fig. 4.

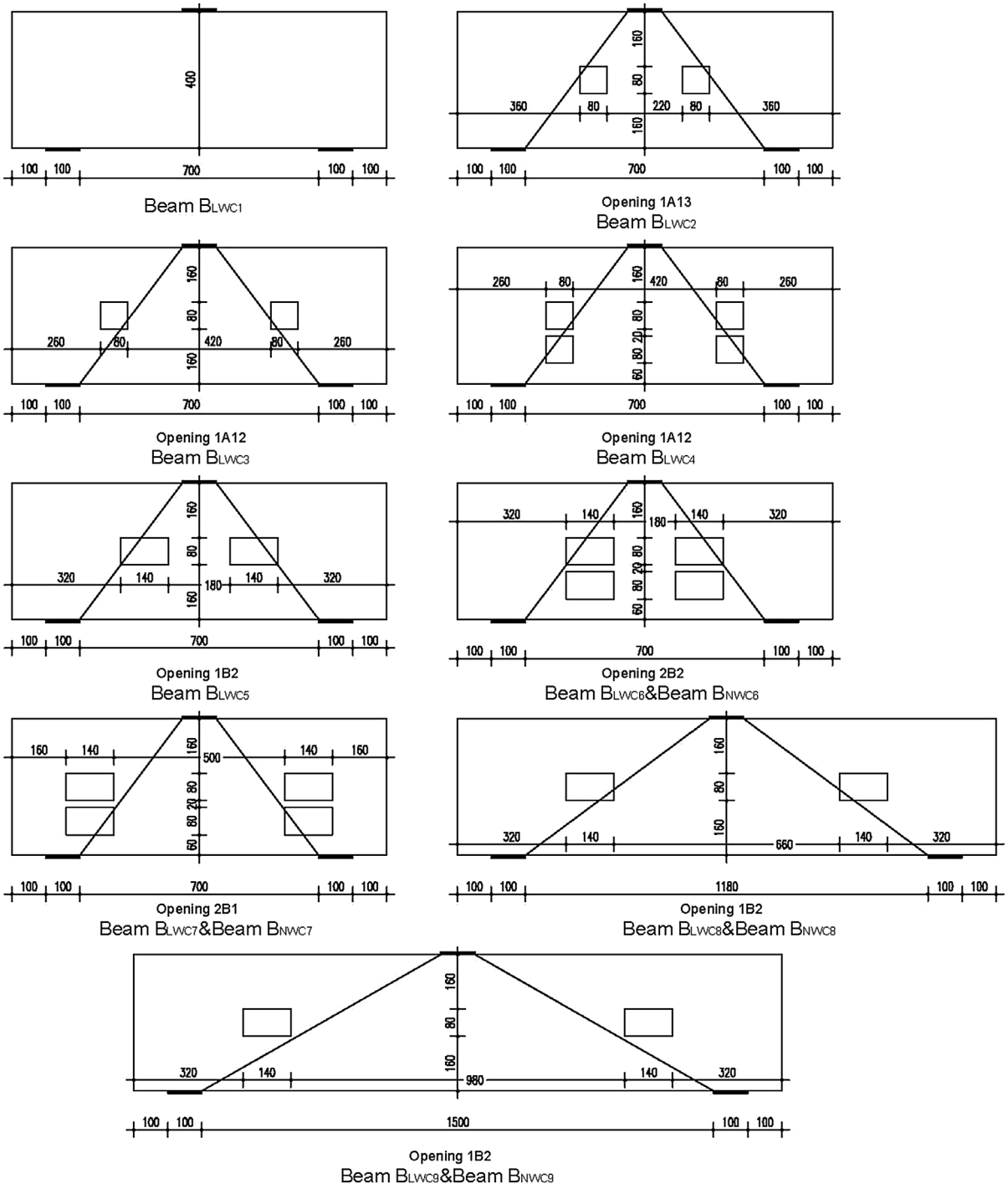


**Fig. 2.** Typical dimensions of tested beam.

For the studied beams with small opening size, $B_{LWC2}$ and $B_{LWC3}$; the first observed cracks were flexural on the tension side at the middle of the beam span. These cracks rapidly propagated with the load increase towards the lower corners of the opening. With the increase of the applied load, shear diagonal cracks were initiated and extended from the support plates to the edges of the openings. At higher loading stages, the width of the main diagonal crack increased as shown in Fig. 4. For

**Table 2**
Mix proportions.

| Concrete type | Cement ($kg/m^3$) | Sand ($kg/m^3$) | Gravel ($kg/m^3$) | w/c ratio | Super-Plasticizer ($liter/m^3$) | Silica fume ($kg/m^3$) | Polystyrene Foam ($liter/m^3$) |
|---|---|---|---|---|---|---|---|
| Light weight | 420 | 630 | 630 | 0.30 | 2.8 | 40 | 330 |
| Normal weight | 350 | 630 | 1260 | 0.5 | – | – | – |

**Table 3**
Mechanical properties of concrete.

| Concrete type | Target $f_{cu}$ ($N/mm^2$) | Cube strength ($N/mm^2$) | | Cylindrical compressive strength ($N/mm^2$) 28 days |
|---|---|---|---|---|
| | | 7 days | 28 days | |
| LWC | 25 | 19.7 | 26.3 | 20.16 |
| NWC | 25 | 17.6 | 25.6 | 19.62 |


**Fig. 3.** Test setup.

these beams, failure occurred above the web opening with inclined cracks starting form loaded plate to the upper corners of the opening. Alsaeq [26] reported similar observations for deep beams with openings.

For the specimens with large openings, $B_{LWC5}$ and $B_{LWC6}$, inclined cracks appeared first from loading point till corner of the upper opening parallel to the compression strut, and then further diagonal cracks were initiated at opening corners. Then, cracks propagated towards loading zone and supports. More diagonal cracks appeared parallel to the strut, passing through the opening corners and propagated towards the loading region and the supporting plates. Three a/d ratio were chosen, the first ratio was 0.97, beam $B_{LWC5}$, the second ratio was 1.63, beam $B_{LWC8}$, and the third ratio was 2.08, beams $B_{LWC9}$. The development of flexural cracks was faster in samples with a large value of a/d ratio; beams $B_{LWC9}$ and $B_{LWC5}$ (see Fig. 4). The recorded ultimate strength of specimen BLWC5 tested at a / d equals 0.97 was more than that of Specimens $B_{LWC8}$ and $B_{LWC9}$ by 11 % and 18 %, respectively. Referring to Figs. 4 and 5, it is clear that the dimensions and position of the openings have major effects on the crack pattern, ultimate strength and failure of studied specimens. This agrees with the findings of Jasim et al. [27] who reported in his experimental and theoretical study of deep beams with a/d ratio equals 1.1 that the large web openings have a great effect on the shear strength of deep beams. It can be seen from the above observations that when the openings interrupt the load path between the loading and reaction points, the crack path changes to a more complex one. It is worth mentioning that failure of all tested specimens was shear failure as shown in Fig. 4).

### *3.2. Cracking loads and ultimate loads*

Fig. 5 displays the cracking loads and ultimate loads of the studied specimens. It can be seen that the cracking load of LWC specimens, $B_{LWC6}$, $B_{LWC7}$, $B_{LWC8}$ and $B_{LWC9}$, are nearly equal to the cracking load of NWC specimens, $B_{NWC6}$, $B_{NWC7}$, $B_{NWC8}$ and

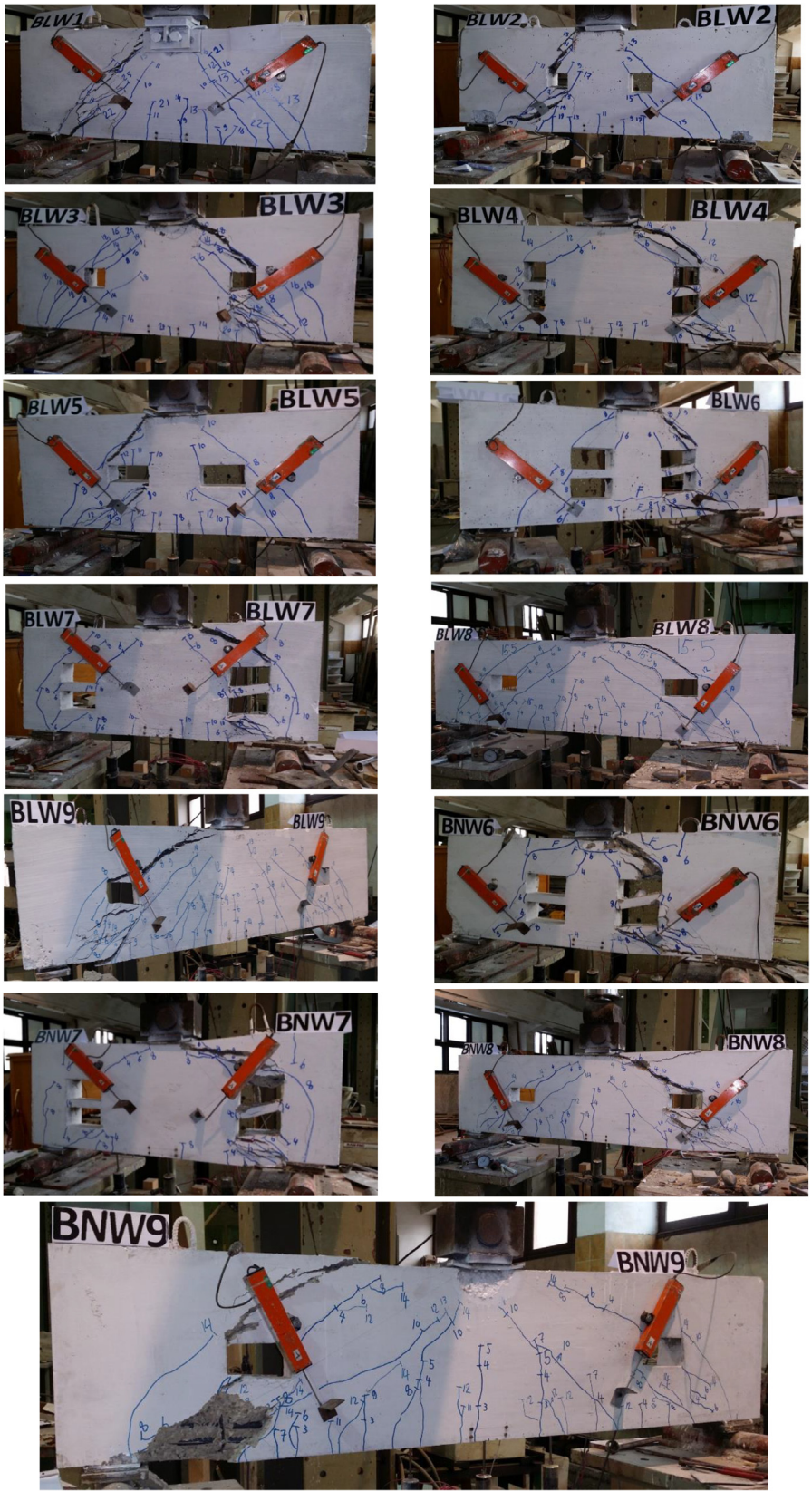


**Fig. 4.** Crack pattern and failure of tested deep beams.

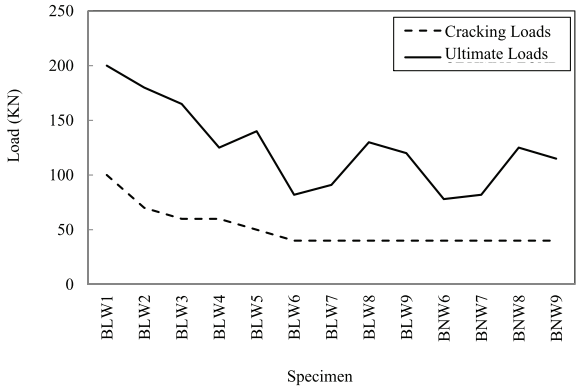


**Fig. 5.** Crack and ultimate load of tested deep beams.

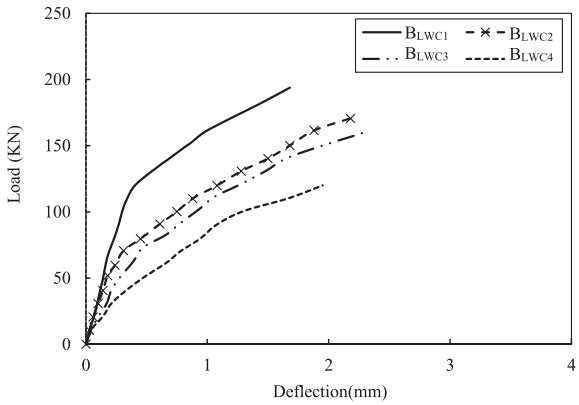


**Fig. 6.** Effect of small opening on load-midspan deflection of specimens.

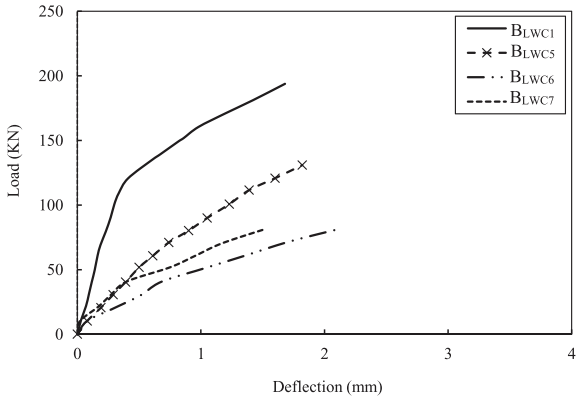


**Fig. 7.** Effect of wide opening on load-midspan deflection of specimens.

$B_{NWC9}$. On the other hand, ultimate loads of LWC specimens were approximately 90–96% of the ultimate loads of NWC counterparts. The cracking load of specimens $B_{LWC2}$, $B_{LWC3}$ and $B_{LWC4}$ was 70 %, 65 %, and 60 % of the cracking loads of solid specimens. As far as the specimens with double rows of openings of depth, 40 %, of the beam depth, the ultimate loads of specimens $B_{LWC6}$ and $B_{LWC7}$ were approximately 41 % and 46 % of the ultimate load of the solid specimen $B_{LWC1}$. Generally, increasing the width of the opening in the shear zone led to drop in the ultimate load of the specimens. The ultimate load of specimens $B_{LWC6}$ was 66 % of that $B_{LWC4}$. It should be noted that the dimensions and position of the web opening have significant effect on the mode of failure and ultimate strength of LWC and NWC deep beams. The presence of openings in the shear span considerably reduced the ultimate strength of the specimens. Similar observations were reported by [2], who

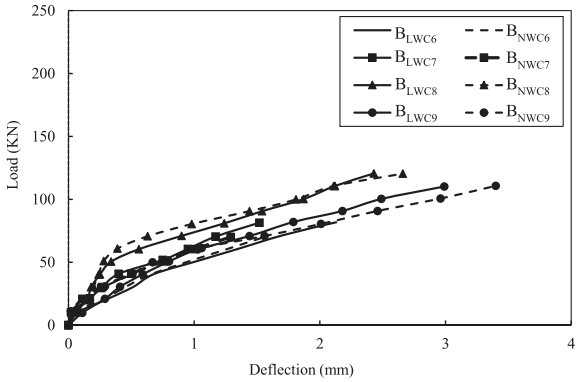


**Fig. 8.** Effect of concrete types on load-midspan deflection of specimens.

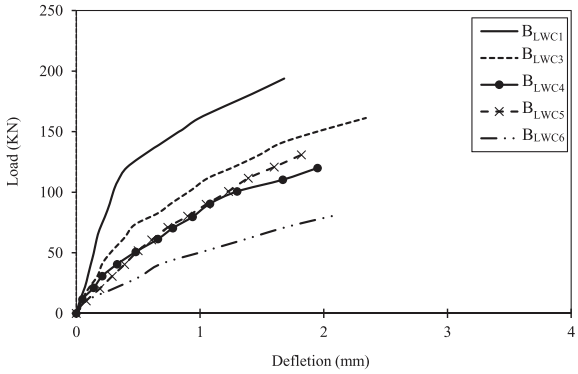


**Fig. 9.** Effect of number of rows of openings on the load-midspan deflection of specimens.

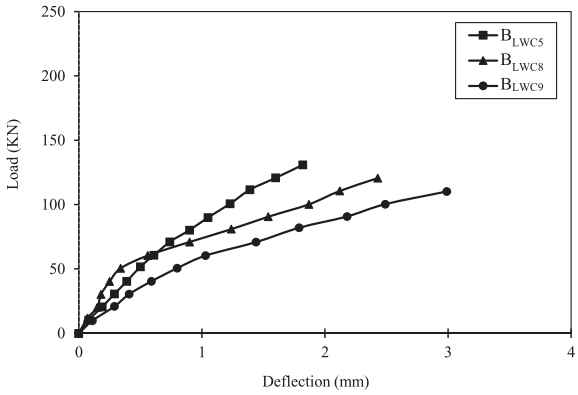


**Fig. 10.** Effect of shear span to depth ratio on the load-midspan deflection of specimens.

found that the ultimate shear strength of HSC deep beams with openings reduced rapidly with the presence of openings in the shear span.

### *3.3. Load-midspan deflection of test specimens*

The deflection at mid-span was measured and recorded at each load increment during testing of each beam. Load-deflection relationships are shown in Figs. 6–10 for all test beams. It can be seen from Fig. 6 that for specimen $B_{LWC1,}$ the beams behaved in a truly elastic manner at early stages of loading. In addition, beams with small web openings; $B_{LWC2}$ and $B_{LWC3}$ showed load deflection behavior very similar to that of the solid beam. Fig. 7 shows that the ultimate load of specimens decreased with increasing the size of openings. It was noticed also that specimens with small openings, $B_{LW2}$, $B_{LW3}$, and $B_{LW4}$

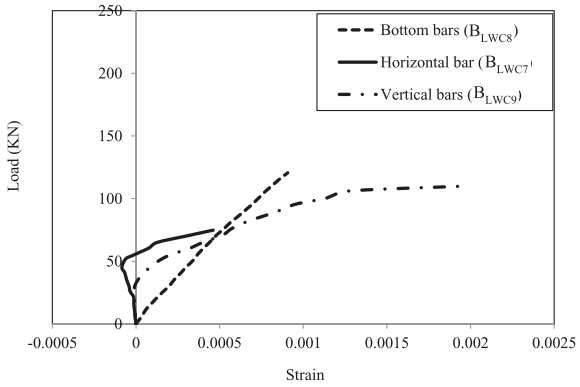


**Fig. 11.** Strain in steel reinforcement of different studied specimens.

**Table 4**
Experimental and finite element analysis results.

| Group | Beam | Experimental | | NLFEA | | NLFEA / Experimental | |
|---|---|---|---|---|---|---|---|
| | | Ultimate load (2Vu) KN | Deflection mm | Ultimate load (2Vu) KN | Deflection mm | Ultimate load ratio | Deflection ratio |
| 1 | $B_{LWC1}$ | 193.81 | 1.42 | 185.00 | 1.36 | 0.95 | 0.96 |
| | $B_{LWC2}$ | 170.64 | 2.18 | 170.00 | 2.03 | 1.00 | 0.93 |
| | $B_{LWC3}$ | 162.00 | 2.34 | 155.00 | 2.20 | 0.95 | 0.94 |
| | $B_{LWC4}$ | 122.00 | 1.95 | 117.00 | 1.89 | 0.96 | 0.97 |
| 2 | $B_{LWC5}$ | 130.89 | 1.98 | 119.75 | 1.92 | 0.92 | 0.97 |
| | $B_{LWC6}$ | 82.00 | 2.13 | 73.50 | 1.81 | 0.89 | 0.85 |
| | $B_{LWC7}$ | 83.00 | 1.5 | 75.00 | 1.49 | 0.90 | 0.98 |
| | $B_{LWC8}$ | 125.00 | 2.43 | 120.00 | 2.37 | 0.96 | 0.97 |
| | $B_{LWC9}$ | 110.25 | 2.99 | 110.00 | 2.87 | 1.00 | 0.96 |
| 3 | $B_{NWC6}$ | 70.00 | 1.56 | 66.80 | 1.55 | 0.95 | 0.99 |
| | $B_{NWC7}$ | 75.00 | 1.29 | 70.00 | 1.34 | 0.93 | 1.04 |
| | $B_{NWC8}$ | 120.45 | 2.66 | 120.00 | 2.02 | 1.00 | 0.75 |
| | $B_{NWC9}$ | 110.66 | 2.96 | 107.26 | 2.81 | 0.97 | 0.95 |

(see Fig. 6) have stiffness higher than those with large openings, $B_{LW5}$, $B_{LW6}$, and $B_{LW7}$, shown in Fig. 7. For example, the ultimate load of $B_{LWC2}$ equals to 1.06 that of $B_{LWC3}$ with opening near the support (see Fig. 6). The effect of concrete type on the mid span displacement for deep beams with web openings is shown in Fig. 8. It can be seen from the figure that the ultimate loads and stiffness of LWC studied beams, $B_{LWC6}$, $B_{LWC7}$, $B_{LWC8}$, $B_{LWC9}$ and their counterparts NWC specimens, $B_{NWC6}$, $B_{NWC7}$, $B_{NWC8}$, $B_{NWC9}$, have a similar pattern. Fig. 9 displays the influence of openings on the reduction of stiffness of the studied deep beams. For example, the ultimate loads of specimens with opening height represent 40 % of the depth of beams, $B_{LWC4}$ and $B_{LWC6}$, were approximately 75 % and 63 % of that of the beams of opening height equals 20 % of the beam depth. For

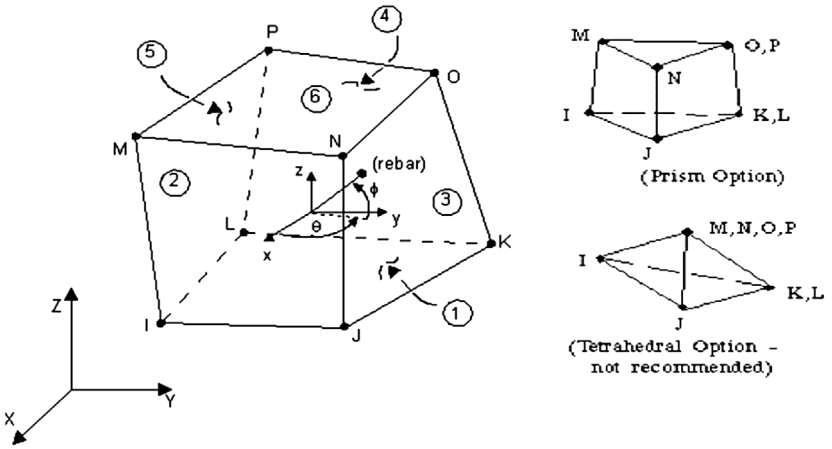


**Fig. 12.** Geometry of 3-D Solid 65 Element (ANSYS 13.0).

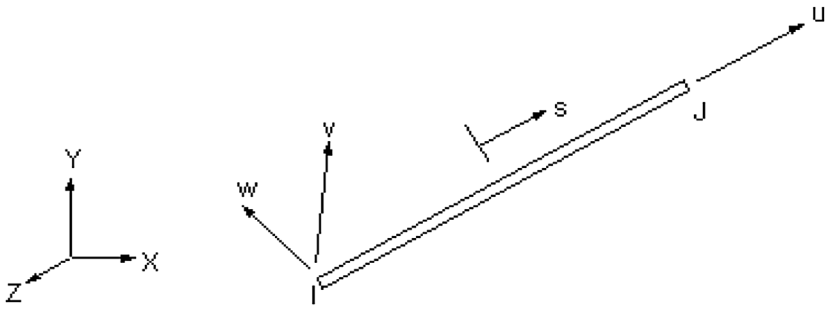


**Fig. 13.** Link8-Element (ANSYS 13).

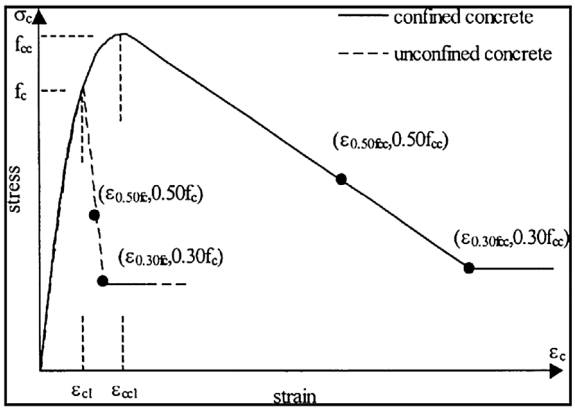


**Fig. 14.** Stress-strain curve for concrete [30].

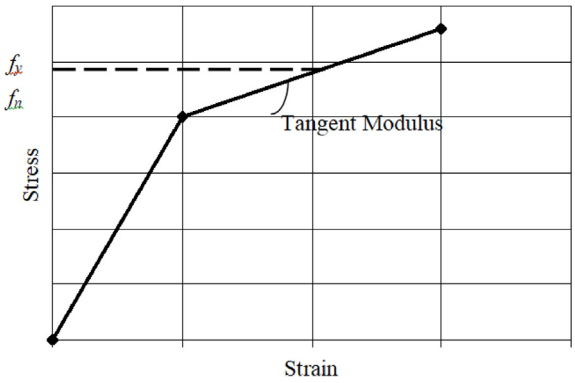


**Fig. 15.** Stress-strain curve for steel reinforcement [31].

$B_{LWC6}$ with large opening (opening size notation, 2B22), the mid span deflection was higher than that of $B_{LWC4}$ with opening size notation, 2A12, and $B_{LWC5}$ with opening size notation, 1B22. This agrees with the findings of Ibrahim et al. [28] who reported the relationship between opening dimensions, position, the stiffness and ultimate capacity. Fig. 10 shows that the reduction in the ultimate load of the studied specimen was 16 % with increasing a/d ratio from 0.97 to 2.08.

### *3.4. Steel strains*

Strain gauges were attached to the tensile steel reinforcement of specimens to examine the disparity of strain in bottom reinforcement. These gauges were attached at mid-span of specimens. Fig. 11 displays a typical measured strain of the specimens. The strain deviation in tensile reinforcement was nearly comparable for all test beams. The development of a tie-action was detected and the strain increased rapidly in the locality of the first crack. Finally, the strains were increased at almost constant loading level until the failure occurred. The maximum strain in flexural reinforcement was less than that of

the yield strain value. The measured strains were ranged from 25 % to 50 % of yield strain of the longitudinal reinforcement. The recorded strain in tension bars showed that the tension failure was protected for all of the specimens to permit for shear failure mode. The maximum recorded strain in longitudinal bars was 0.0009 for Specimen $B_{LWC8}$ (see Fig. 11). Similar load-tensile steel reinforcement strain was observed by Ibrahim et al. [28]. Fig. 11 shows also that the strain in vertical stirrups was recorded at the critical shear locations. Prior to the occurrence of the first crack, the internal shear resistance was provided by the beam section. Once the diagonal cracks occurred, strains of the vertical stirrups were recorded, representing shear resistance role by the vertical stirrups. The maximum strain in vertical stirrups was approximately 0.002 for Specimen $B_{LWC9}$. The yielding of vertical stirrups occurred before failure of deep beams. The maximum horizontal stirrups' strain was 0.00046 for Specimen $B_{LWC7}$ as shown in Fig. 11.

## 4. Finite element modelling of deep beams

The experimentally tested thirteen specimens were numerically modeled using [29]), package to predict their results versus the experimental results for the main studied parameters, dimension and position of opening, the design concrete compressive strength, the transverse reinforcement ratio, and a/d ratio. Details of the finite element modelling, predictions of the results using the tested model are reported and discussed in the following sections.

### *4.1. Element types, material properties and constitutive models*

Concrete and steel are the two main materials used in the numerical analysis of the deep beam in which their properties and constitutive models are presented. The solid element used in this study was Solid65 which is one of the elements in ANSYS program to model the three-dimensional behavior of concrete. Solid65 was assumed to model the concrete as it is capable of cracking in tension and crushing in compression. The geometrical characteristics of the 3-D Solid65 element are shown in Fig. 12. The element is defined by eight nodes and each node has three degrees of freedom. The flexural and shear reinforcement in the tested beams were idealized using the Link8 element as shown in Fig. 13. The axial stress is assumed to be uniform over the entire element. Full bond was assumed between concrete and reinforcing steel. Both linear and non-linear behaviors of the concrete were considered. For the linear stage, the concrete is assumed to be an isotropic material up to cracking. For the non-linear segment, the concrete may undergo plasticity. The numerical solution scheme adopted for non-linear analysis was an incremental load procedure based on the iterative solution using Newton-Raphson method. The convergence criterion currently used was based on the iterative nodal displacement where only transitional degrees of freedom were considered.

#### *4.1.1. Constitutive modeling for concrete*

The concrete material model assigned for Solid65 element used throughout this study is characterized by its capability to predict the failure of brittle materials. Both cracking and crushing failure modes are accounted for. The criterion for failure of concrete due to a multi-axial stress state can be expressed in the form:

$$\frac{F}{f_c} - S \geq 0 \tag{1}$$

To model concrete behavior, nonlinear stress-strain curves were used in compression and tension [30]. Such models account for compression & tension softening, tension stiffening and shear transfer mechanisms in cracked concrete as presented in Fig. 14.

#### *4.1.2. Constitutive modeling for steel*

The average stress-strain curve developed earlier by Soroushian and Lee [31] for steel bars embedded in concrete is used in the current research (see Fig. 15). The stress-strain relationship is expressed by two straight lines as follows:

For $\varepsilon_s \leq \varepsilon_n$:

$$f_s = E_s \varepsilon_s \tag{2}$$

and for $\varepsilon_s \geq \varepsilon_n$:

$$f_s = f_y \left[ (0.91 - 2B) + \left( 0.02 + 0.25B \frac{\varepsilon_s}{\varepsilon_y} \right) \right] \tag{3}$$

Where $\varepsilon_n = \varepsilon_y (0.93 - 2B)$.

And the parameter B is given as $\left( f_{cr}/f_y \right)^{1.5} / \rho$.

The recommended value of $f_{cr}$ is given as:

$$f_{cr} = 0.31 \sqrt{f_c'} \text{In MPa} \tag{4}$$

*4.1.3. Modelling of simple deep beams*

The beams are modeled using nonlinear solid element (solid 65) and Link 8 -3D bars. The cross section is divided into five strips according to the main bottom and top as shown in Fig. 16. Strip (S1) is 20 mm thick and represents the concrete cover at the bottom of beam section only. The second strip (S2) is (30 mm) thick and represents the concrete part at the bottom of the beam section that contains two bars of the main reinforcement (4 Ø 16) and represents the upper part of concrete that contains the top secondary steel (2 Ø 10) reinforcement in that part of the upper concrete cover. Longitudinally, the distance between point load and support is meshed with twenty-two strips (50 mm × 22). In addition, a finer mesh was generated under the point loads and supports (20 mm (4 × 20 mm) for different beams) as shown in Fig. 17 for typical studied beams. Three stiff reinforced concrete solid elements were meshed and used to model the two supports and the point load as shown in Fig. 17. The two-hinged supports are located at the lower parts of the reinforced concrete elements. The point load was represented by five nodes of the reinforced concrete elements.

*4.2. Finite element results*

*4.2.1. Prediction of crack patterns and failure mode*

Fig. 18 shows a comparison between finite element prediction and experimentally observed crack patterns for selective specimens, which were previously introduced in Fig. 5. In addition, Table 4 shows the predicted values for the ultimate loads and corresponding deflection for the studied beams. It can be seen from Fig. 18 that the crack patterns for deep beams predicted by finite element model are in good agreement with the experimentally observed ones. At approximately 43 % of the ultimate load of capacity of specimens, a rapid main inclined tension crack formed nearly in the middle part of the shear span. In addition, inclined cracks spread to the beam support. For beams with openings, the cracks spread above openings to the point load. Then the crack extended down from the openings to supports. Finally, failure occurred in opening region. Compression stresses were concentrated along the load path. The tensile stresses were eliminated in the finite element analysis generating cracks in concrete and they were relocated to steel crossing this region. The stress level depends mostly on the dimension and position of the opening. In addition, the concrete strength has a greater effect with a decreasing a/d ratio. The higher compressive stresses occurred at nodal zones, whilst a reduction in the compressive stresses occurred in the inclined struts linking the points load and supports. This reduction is due to the opening in the load path. Fig. 19 displays the deformed shape and vertical displacement before failure for selected beams. The above comparison shows also that the ultimate load of LWC is slightly higher than that of NWC and this may be attributed to the fact that actual concrete cube strength for LWC specimens was slightly higher than that of NWC companions in this study.

*4.2.2. Prediction of Load-deflection relations*

Fig. 20shows comparisons between experimental load-deflection relationships and those predicted numerically. In addition, Table 4 shows comparisons between experimental and numerical results for ultimate loads and corresponding

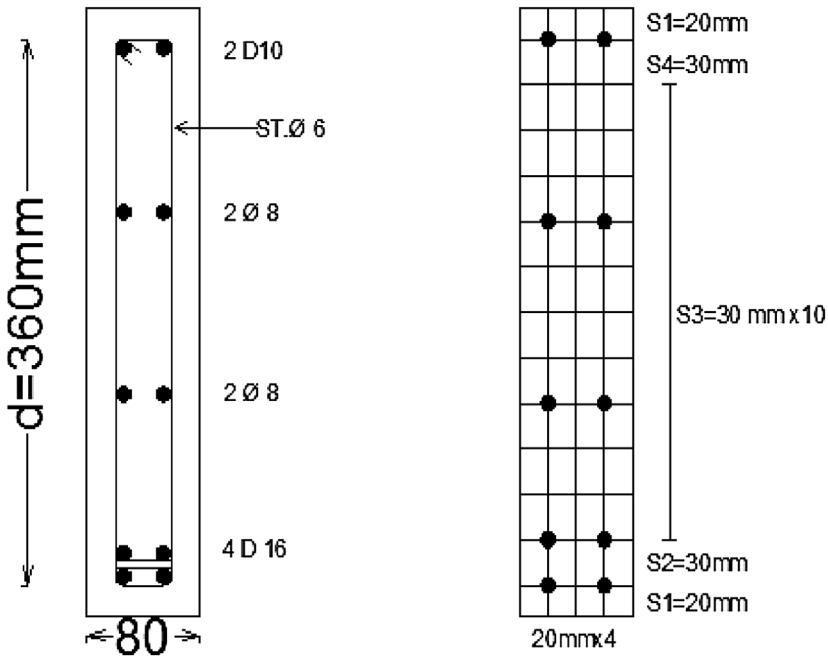


**Fig. 16.** Meshing of cross section.

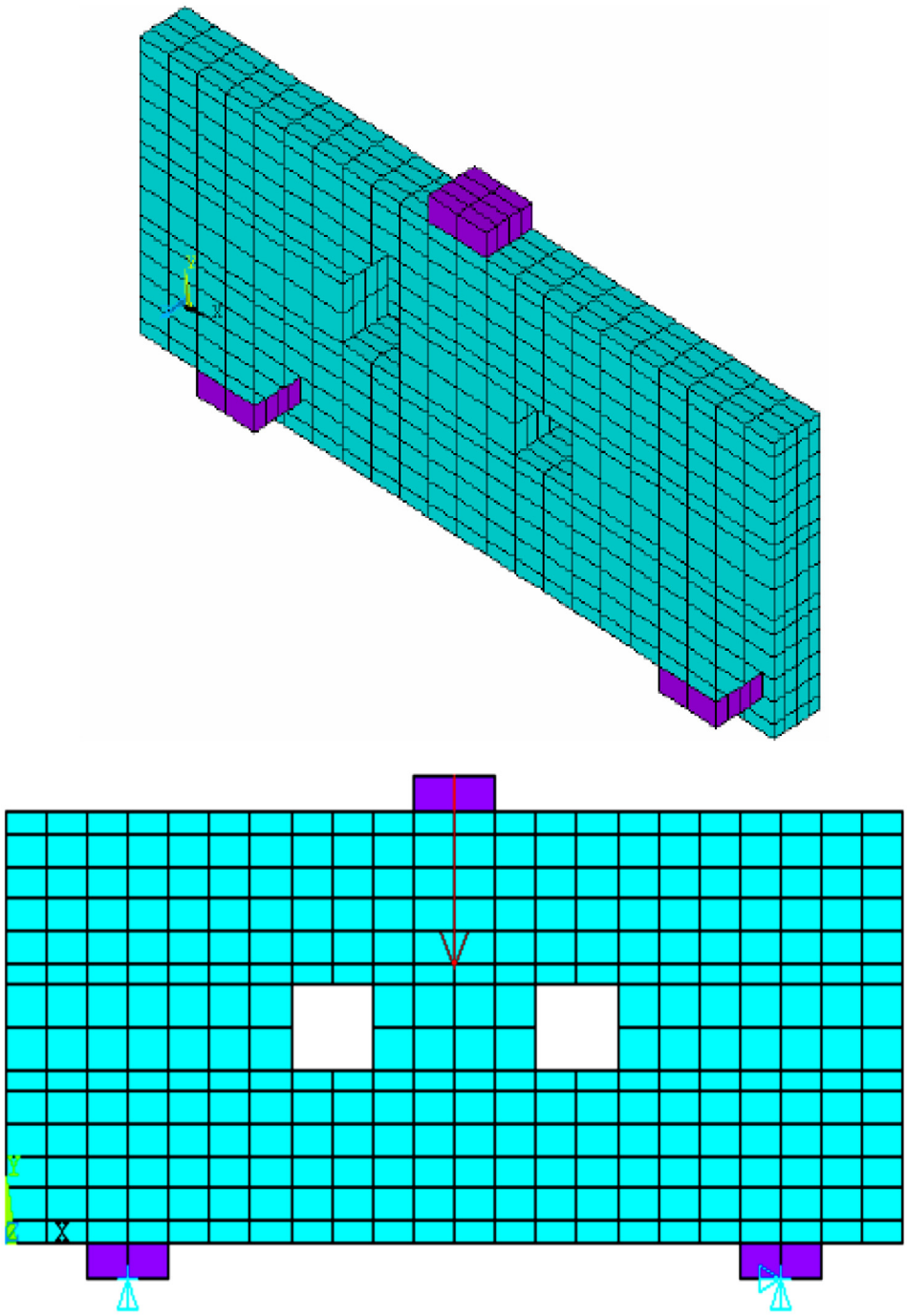

**Fig. 17.** Meshing, loading and boundary conditions of a typical studied beam.

deflection. Fig. 20 and Table 4 reveal that there is a very good agreement between the numerical and the experimental test results. The ratio of the predicted ultimate loads to the experimental ones for the tested deep beams ranged between 0.89-1.0.

*4.2.3. Parametric study (Effect of interior strengthening)*

A parametric study was carried out by adding more parameters, other than those used in the experimental study in this research, to examine the performance of LWC deep beams with openings having different configurations. The extra studied parameters reported in Table 5 were changing the bottom (tensile) reinforcement ratio for solid deep beams and those with openings, adding top and bottom reinforcement adjacent to the edges of the opening, adding right and left reinforcement

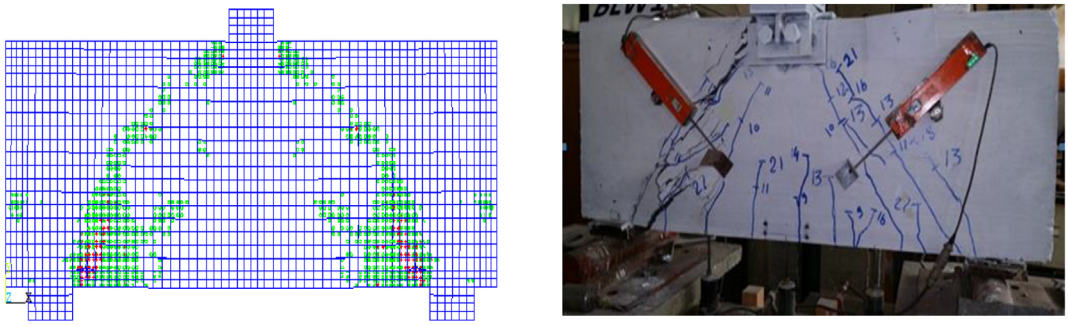

$B_{LWC1}$

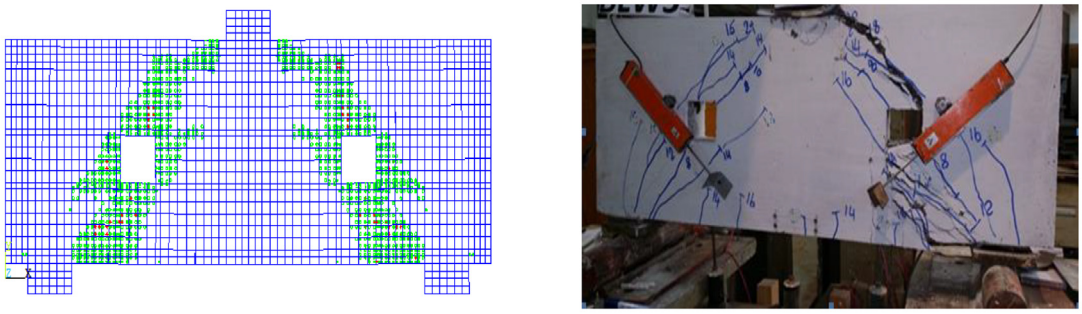

$B_{LWC3}$

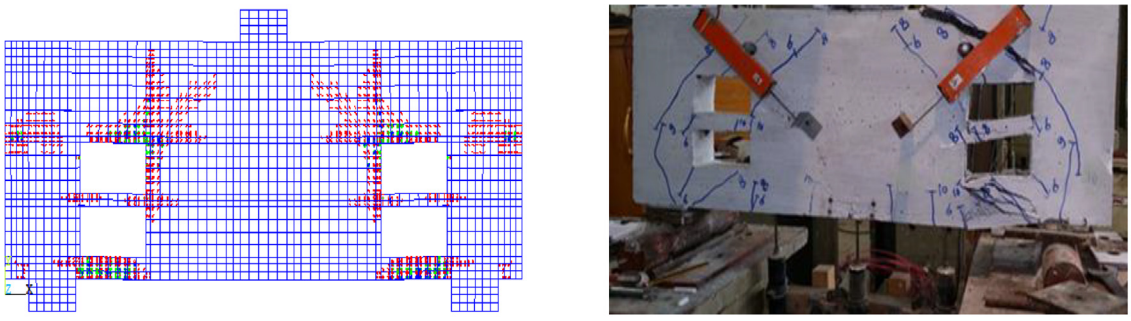

$B_{LWC7}$

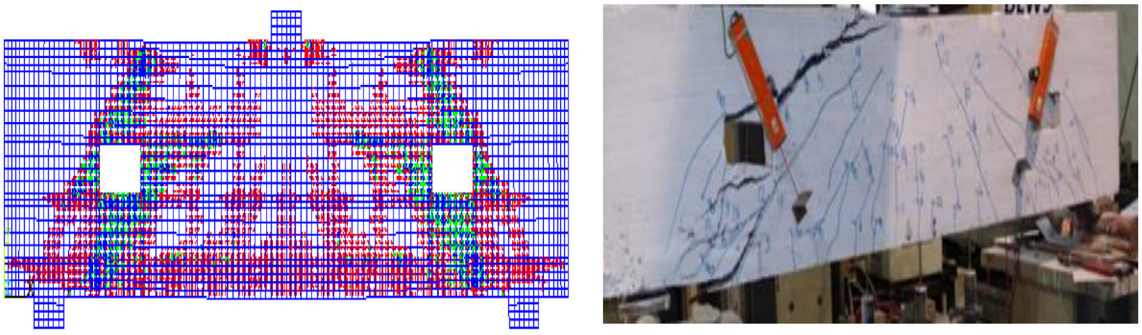

$B_{LWC9}$

**Fig. 18.** Comparison between predicted and experimental crack pattern and failure modes for selected beams.

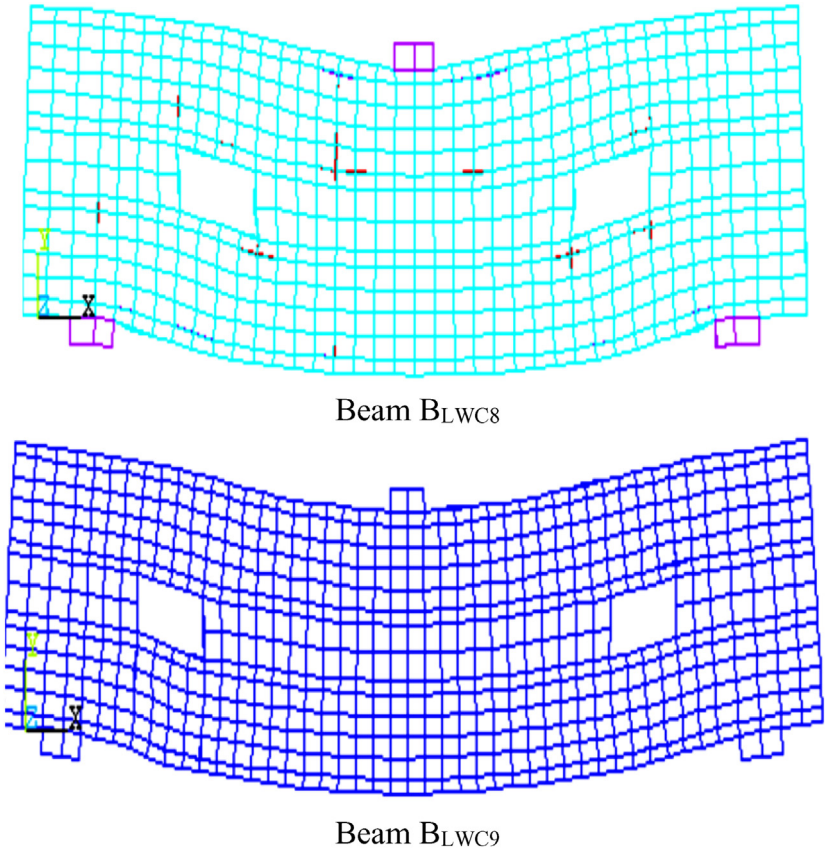


**Fig. 19.** Deformed shape of selected beams.

adjacent to the opening edges, and adding reinforcement at all sides of the opening. It is worth mentioning that the opening notation is the same as that for experimentally tested beams in Table 1. Fig. 21a shows the numerical load-deflection for solid deep beam specimens with different bottom reinforcement. It can be seen from the figure that the increase of longitudinal bottom reinforcement led to a reasonable increase in the ultimate capacity. For example, Specimen DA3 of higher tensile reinforcement ratio of 0.54 % (4Ø22 bottom reinforcement) exhibited more ductile behavior compared to that of specimen DA1 of 0.16 % tensile reinforcement ratio (4Ø12 bottom reinforcement). The increase in ultimate load of specimens DA3 was approximately 18 %. The same change in bottom reinforcement was applied to Specimens, DC1, DC2, and DC3 as indicated in Table 5. Fig. 21b shows the load- deflection relationships for those specimens. The tensile steel reinforcement has a profound effect on the post-peak response of these LWC specimens. The maximum increase in the ultimate load was 11 % as the tensile reinforcement ratio increased from 0.16 % (4Ø12) to 0.54 % (4Ø22).

Fig. 21c shows that, Specimens DK2 and DK3, provided with additional steel reinforcement above and below opening, exhibited more ductile behavior compared to that of Specimen DC2, which had no additional reinforcement. The increase in ultimate load of Specimens DK2 and DK3 was approximately 9 % and 15 %, respectively. Adding 2Ø16 additional reinforcement for Specimen DK3 above and below the opening led to an increase in the ultimate deflection by 30 % over that of Specimen DC2, which has no additional reinforcement around edges of the opening. Fig. 21d shows load deflection relationships for specimens with additional vertical bars left and right the opening. The enhancement in the ultimate load was 13 % and 23 %, for Specimens DR2 and DR3 over that of Specimen DC2, which has no additional reinforcement. Fig. 21e shows the load-deflection relationships for specimens provided with additional reinforcement at all sides. It can be seen from the figure that the load carrying capacity increases with increasing addition reinforcement around all side of the opening. For example, the increase in the ultimate load and corresponding ultimate deflection for Specimen DY2 were 18 % and 12 %, compared to those of Specimen DC2, which has no additional reinforcement. In addition, the increase in the ultimate load and corresponding ultimate deflection of Specimen DY3 were 30 % and 28 % over those of Specimen DC2, which has no additional reinforcement. The parametric results showed that adding additional reinforcement around the openings could be considered as internal stiffening of the beams around openings.

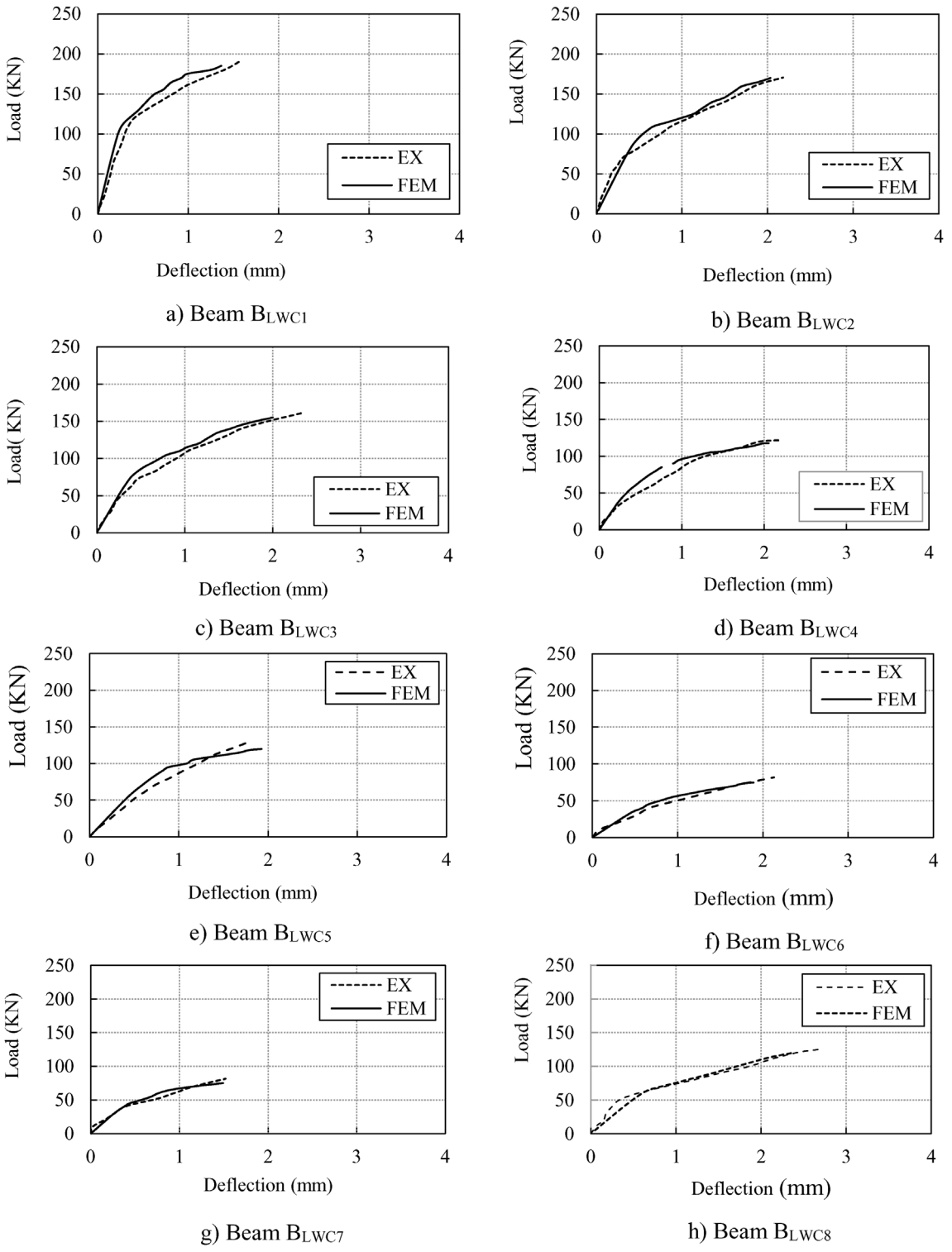


**Fig. 20.** NLFEA and experimental Load-deflection for tested deep beams.

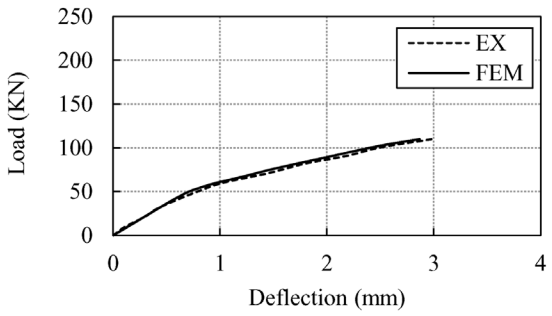


i) Beam $B_{LWC9}$

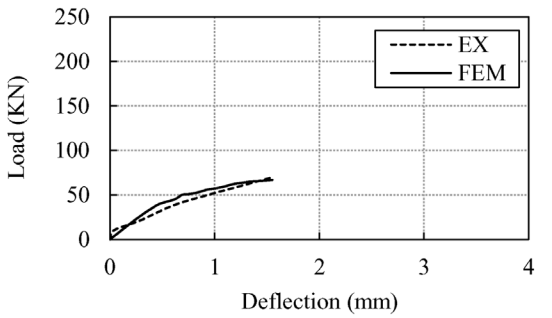


j) Beam $B_{NWC6}$

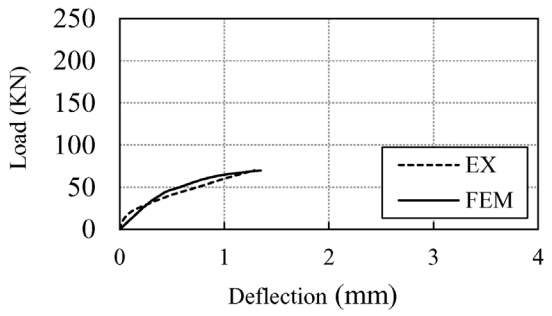


k) Beam $B_{NWC7}$

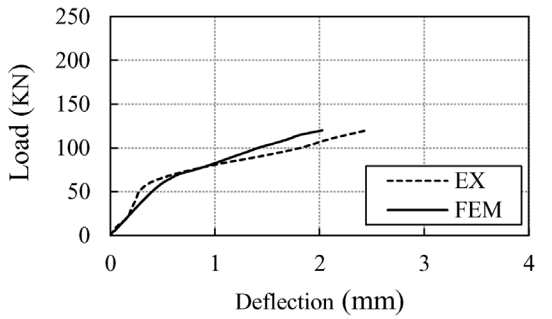


l) Beam $B_{NWC8}$

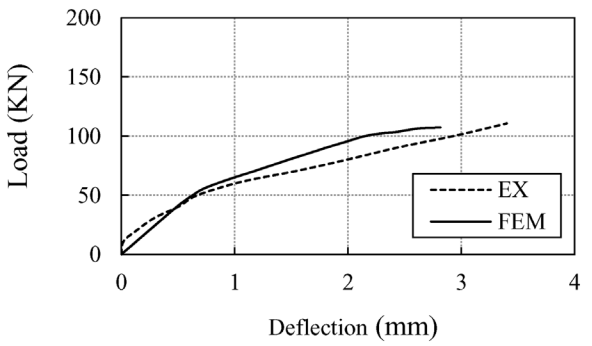


m) Beam $B_{NWC9}$

**Fig. 20.** (Continued)

## 5. Rational prediction of results (Strut-and Tie-modelling)

Most of Strut-and-tie models (STM) for simple deep beams with openings in literature are based on experimental results for crack patterns and modes of failure [32–36]. In the current research, the STM was applied to the studied specimens similar to the analysis carried out earlier by Foster and Lan Gilbert [25]; [34]; El-Demerdash et al. [36] who had single midspan loading (Type I) which is similar to the applied loads in the current research. Fig. 22 shows a simple deep beam with a single top point load at its mid-span along with the proposed Strut-and-Tie model (Fig. 22a). The model has two concrete struts, S, one tension tie T, and three nodes N1 and N2 (Figs. 22b and c). The load transferred directly from point load to support through the concrete, S (Fig. 22c). The steps for solving the beams by the numerical procedure for one concentrated point Loads is detailed as follows:

(a) Input data

The terms of beam size (h, b, $b_1$, and $b_2$), (a/d), and the used concrete and reinforcement strength ($f'c$, and $f y$) are known as input data.

**Table 5**
Parametric study using ANSYS.

| Numerically Studied Beams Notation | Openings Notation | Steel Reinforcement | | Openings additional Top & bottom reinforcement | Openings additional left and right reinforcement |
|---|---|---|---|---|---|
| | | Bottom | Top | | |
| DA1 | – | 4Ø12 | 2Ø10 | – | – |
| DA2 | – | 4Ø16 | 2Ø10 | – | – |
| DA3 | – | 4Ø22 | 2Ø10 | – | – |
| DC1 | 1A12 | 4Ø12 | 2Ø10 | – | – |
| DC2 | 1A12 | 4Ø16 | 2Ø10 | – | – |
| DC3 | 1A12 | 4Ø22 | 2Ø10 | – | – |
| DK2 | 1A12 | 4Ø16 | 2Ø10 | 2Ø12 | – |
| DK3 | 1A12 | 4Ø16 | 2Ø10 | 2Ø16 | – |
| DR2 | 1A12 | 4Ø16 | 2Ø10 | – | 2Ø12 |
| DR3 | 1A12 | 4Ø16 | 2Ø10 | – | 2Ø16 |
| DY2 | 1A12 | 4Ø16 | 2Ø10 | 2Ø12 | 2Ø12 |
| DY3 | 1A12 | 4Ø16 | 2Ø10 | 2Ø16 | 2Ø16 |

(a) The internal lever arm $L_d$

$$a_1 = 2(c+\phi_{str}) + \sum_{i=1}^{n} \phi_i + s \tag{5}$$

Thus

$$L_d = h - 0.50(a_1 + a_2) \tag{6}$$

And $a_2 = 0.80a_1$

(a) Inclination of strut S

$$\alpha = \tan^{-1}\frac{L_d}{a} \tag{7}$$

(a) Strut widths $W_{1av}$ and $W_2$:

From the details of node $N_1$, shown in Fig. 22c, $W_{11}$ may be obtained from:

$$W_{11} = a_1\cos\alpha + b_1\sin\alpha \tag{8}$$

from equilibrium of truss forces,

$$T = S\cos(a) \tag{9}$$

At node 1

$$T = 0.80\, f_c\, a_1\, b \tag{10}$$

Where the value (0.80), represents the effectiveness factor of the nodal zone ($\nu_n$) [25] at node $N_2$:

$$S\cos\alpha = 1.0 f_c a_2 b \tag{11}$$

Where the value (1.0), represents the effectiveness factor of the nodal zone ($\nu$).

$a_2 = 0.8\ a_1$

Also, from the geometry of node $N_2$, $W_{12}$ is given by:

$$W_{12} = a_2\cos\alpha + \frac{b_2}{2}\sin\alpha \tag{12}$$

$$W_{1a\nu} = \frac{W_{11} + W_{12}}{2} \tag{13}$$

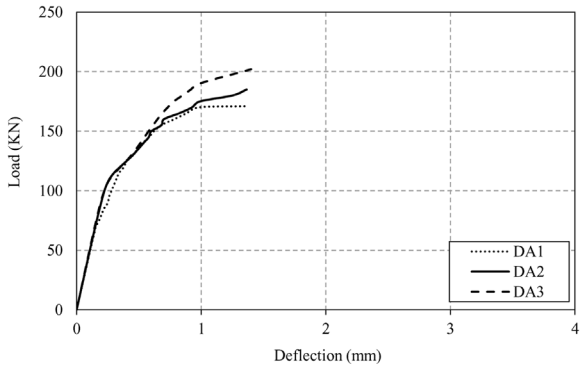


(a) Effect of tensile steel reinforcement (solid deep beams)

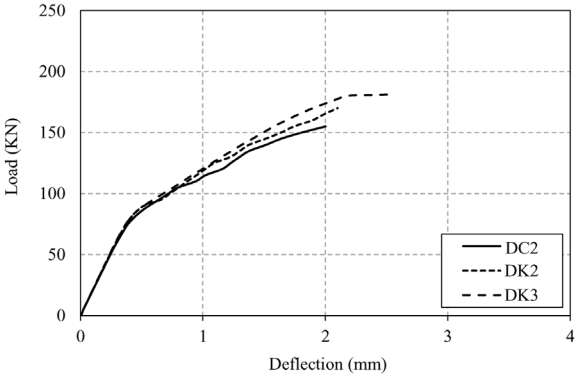


(c) Effect of additional reinforcement at top and bottom of opening

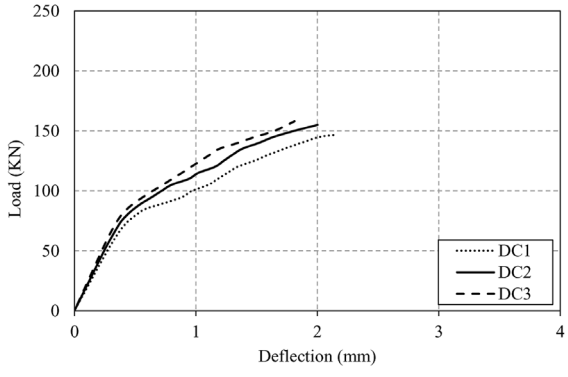


(b) Effect of tensile steel reinforcement (deep beams with openings)

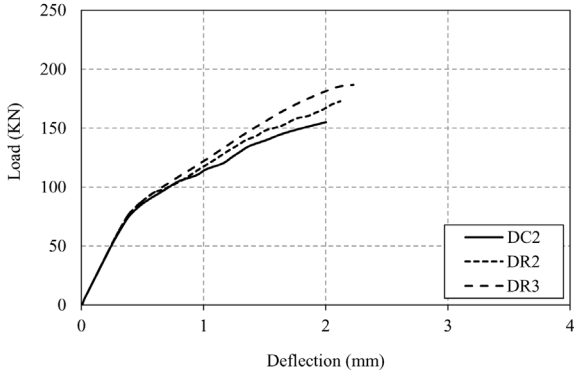


(d) Effect of additional reinforcement at left and right sides of the opening

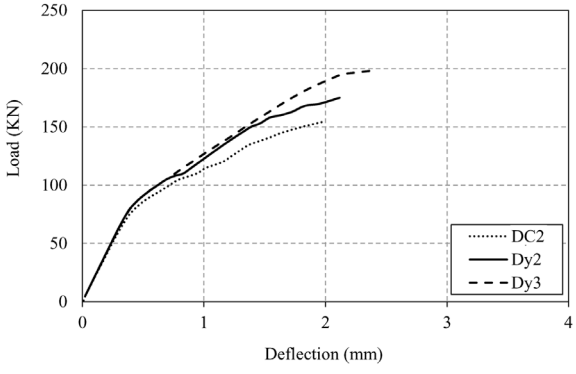


(e) Effect of additional reinforcement at all sides of the opening

**Fig. 21.** Parametric study for the effect of tensile and additional reinforcement on the load-midspan deflection relationships.

(a) Truss forces

Assuming that the steel bars reach their yield strength ($f_s = f_y$), the compressive and tensile forces in the truss members are as follows:

$$T = A_s f_y \quad (14)$$

$$V = S \sin\alpha \quad (15)$$

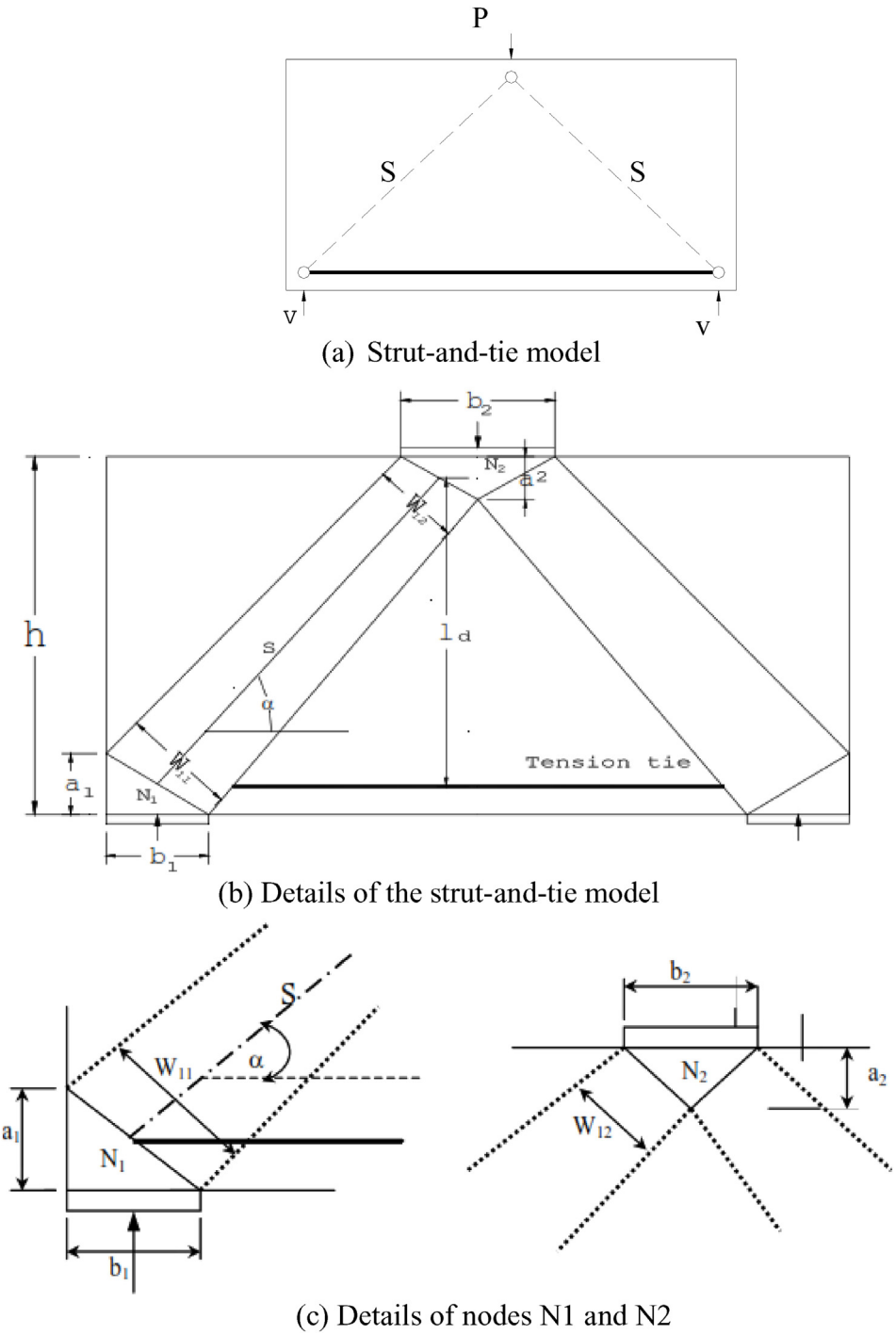


**Fig. 22.** Symbols and details of Type I model for simple deep beam subjected to single point load.

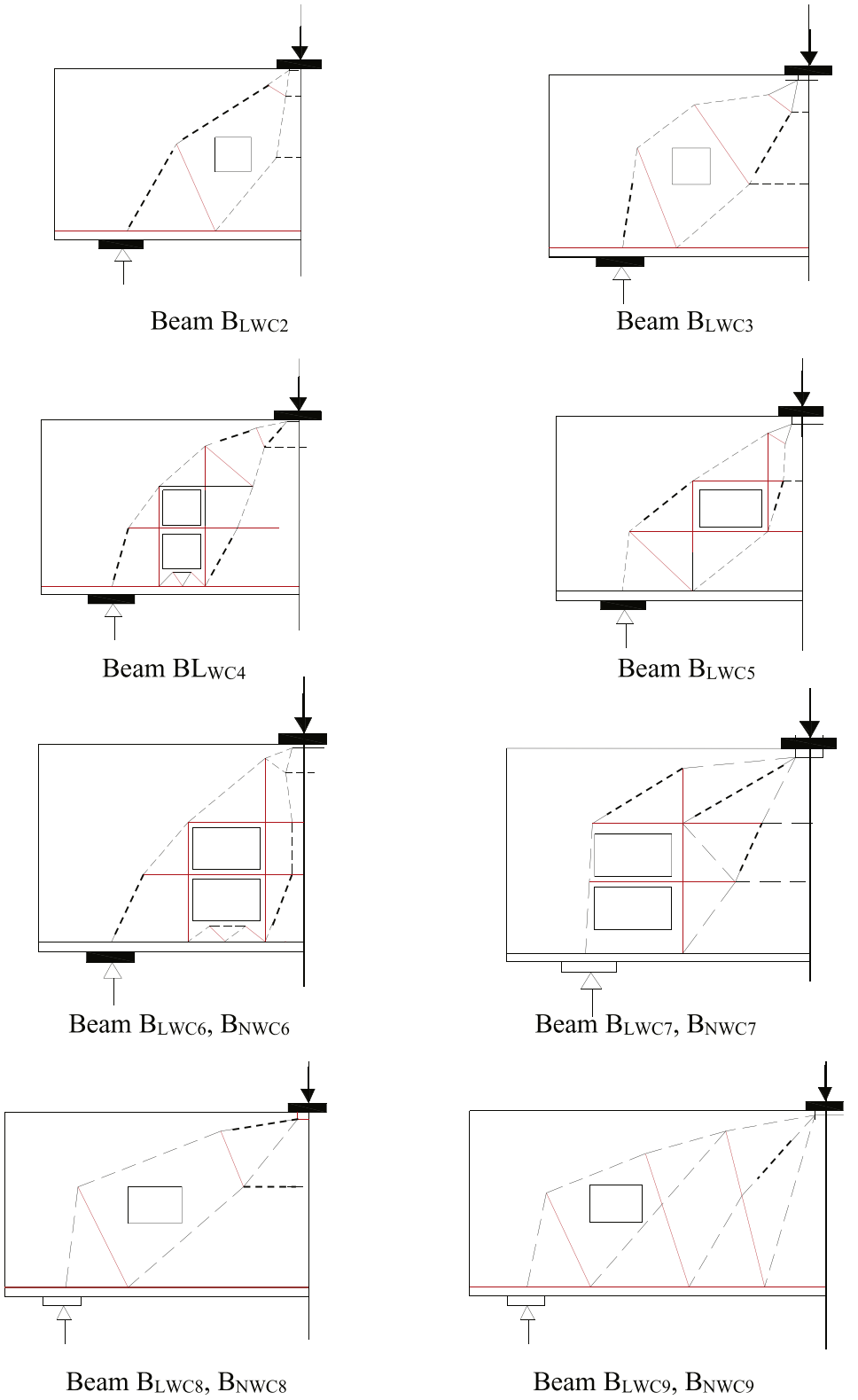


**Fig. 23.** Strut-and-tie modelling for test beams with openings.

**Table 6**
Prediction of experimental results using the strut-and-tie model.

| Group | Beam | ($2Vu_{exp}$) KN | ($2Vu_{STM}$) KN | $Vu_{STM}$ / Vuexp |
|---|---|---|---|---|
| 1 | $B_{LWC1}$ | 193.81 | 155 | 0.80 |
| | $B_{LWC2}$ | 170.64 | 133.1 | 0.78 |
| | $B_{LWC3}$ | 162.00 | 147.4 | 0.91 |
| | $B_{LWC4}$ | 122.00 | 93.90 | 0.77 |
| 2 | $B_{LWC5}$ | 130.89 | 92.9 | 0.71 |
| | $B_{LWC6}$ | 82.00 | 51.25 | 0.625 |
| | $B_{LWC7}$ | 83.00 | 48.1 | 0.58 |
| | $B_{LWC8}$ | 125.00 | 100.0 | 0.80 |
| | $B_{LWC9}$ | 110.25 | 69.46 | 0.63 |
| 3 | $B_{NWC6}$ | 70.00 | 49.4 | 0.71 |
| | $B_{NWC7}$ | 75.00 | 50.8 | 0.68 |
| | $B_{NWC8}$ | 120.45 | 100.7 | 0.84 |
| | $B_{NWC9}$ | 110.66 | 79.8 | 0.72 |

(a) Check of the stress limits

- Concrete struts:
The effective concrete compressive strength in the concrete struts can be obtained from:

$$f_{ce} = \nu_s \phi f_c^{'} \tag{16}$$

Where the values of effectiveness factor ($\nu_s$) for struts $S_1$ and $S_2$ are chosen [25], then check if

$$S \le f_{ce}^{s} W_{1av} b \tag{17}$$

- Nodes:
The effective concrete compressive strength in the nodal zones can be obtained from:

$$f_{ce} = \nu_n \phi f_c^{'} \tag{18}$$

Where the values of effectiveness factor ($\nu_n$) for nodes $N_1$ and $N_2$ are chosen [25].
Check the following conditions at node $N_1$:

$$S \le f_{ce}^{N1} W_{11} b \tag{19}$$

$$V \le f_{ce}^{N1} b_1 b \tag{20}$$

$$T \le f_{ce}^{N1} a_1 b \tag{21}$$

$$S \le f_{ce}^{N2} W_1 2b \tag{22}$$

$$P \le f_{ce}^{N2} b_2 b \tag{23}$$

If the above-mentioned checks are satisfied, the required ultimate shear capacity can be obtained.

The proposed (STMs) for tested deep beams are plotted in Fig. 23 where the dotted lines indicate the compression members while continuous lines indicate the tension members. All the experimentally tested beams were solved using STM approach using the steps in the above equations and the models for tested beams are detailed in Fig. 23. Results obtained by the STM are recorded in Table 6. It can be seen from Table 6 that the STM underestimates the shear of the studied beams compared to experimental results for different tested beams. In addition, the experimental results were in acceptable agreement with those obtained using STM in most cases. Moreover, comparing the results in Table 4 with those in Table 6 shows that the finite element results are more accurate than those obtained by STM. However, the STM can be used as a rational approach for the analysis of LWC deep beams with openings which contain polystyrene balls as coarse aggregates.

## 6. Conclusions

This paper covers the gap in the literature since it contains more studied variables such as partial replacement of coarse aggregate by polystyrene foam balls, the number of openings, web reinforcement ratio and positioning the openings in shear zone. The authors carried out experimental work, finite element technique, and rational STM approach in this research to study the shear behavior of studied beams subjected to single midspan concentrated loads. The following conclusions can be drawn from this study:

1 The overall weight of deep beams containing polystyrene foam balls as partial replacement of coarse aggregate was less than their counterparts of NWC deep beams by approximately 30 % while their shear behavior and mode of failure were almost similar to their counterparts of NWC ones. This is very interesting and promising to build lighter deep beams with efficient structural behaviour.
2 Shear span-to-depth ratio (a/d) has a considerable effect on the cracking and the ultimate shear strength of deep beams with openings. The development of initial flexural cracks was more rapid in specimens with a larger value of shear-span-to depth ratio. Increasing a/d ratio from 0.97 to 2.08 led to reduction of the cracking and the ultimate shear strengths by approximately 50 % and 12 %, respectively.
3 The presence of openings in the shear span considerably reduced the ultimate strength of the specimens. Size of the web openings has a major impact on the failure mode and ultimate shear strength of reinforced LWC deep beams. Increasing the depth of the opening from 20 % to 40 % of the total beam depth led to reduction in the ultimate load by 28 % and 46.4 % compared to that of similar solid deep beams.
4 Locating the opening in mid shear span zone leads to a high reduction in shear strength. Increasing the width of the opening in the shear zone led to reduction of the ultimate load of the specimens up to 66 %.
5 Application of finite element modelling to test beams, yielded very good prediction of load-carrying capacities, cracking pattern and load-deflection relationships.
6 The parametric study carried out by finite element showed that increasing tensile steel reinforcement ratio (bottom reinforcement) led to an increase of the ultimate shear capacity and ultimate displacement. In addition, internal stiffening of the beams around openings increased the shear capacity and the displacement ductility. The enhancement of shear capacity was approximately up to 30 %.
7 Prediction of experimental results using strut-and-tie model was carried out successfully and the agreement was acceptable in most cases but the finite element results were more accurate than those obtained by STM. However, the STM can be used as a rational approach for the analysis of LWC deep beams with openings which contain polystyrene balls as coarse aggregates.
8 Based on the results of this research, it is recommended that the depth of opening should not exceed 20 % of the deep beam depth. If the depth of opening is more than that or lies in the shear span it is highly recommended for strengthening the opening internally by additional reinforcement around perimeter of the opening.

## Declaration of Competing Interest

This is to declare that all the authors have no conflict of interest.

## Acknowledgement

October 6 Universities is acknowledged for funding this research project. The experimental work was carried out in the reinforced concrete laboratory at Ain Shams University. Technicians and staff are acknowledged for their valuable assistance.

## References

[1] I.G. Shaaban, Structural behaviour of reinforced concrete deep beams with and without openings, Civ. Eng. Res. Mag. (CERM) 21 (4) (1999) 879–899 Al-Azhar University, Cairo, Egypt.
[2] K.-H. Yang, H.-C. Eun, H.-S. Chung, The influence of web openings on the structural behaviour of reinforced high-strength concrete deep beams, Eng. Struct. 28 (13) (2006) 1825–1834.
[3] M. Haque, Rasheeduzzafar, A.H. Al- Tayyib, Stress distribution in deep beams with web openings, J. Struct. Eng. 112 (5) (1986) 1147–1165.
[4] T. El Maaddawy, S. Sherif, FRP composites for shear strengthening of reinforced concrete deep beams with openings, Compos. Struct. 89 (1) (2009) 60–69.
[5] S. Amiri, R. Masoudnia, M.A. Ameri, A review of design specifications of opening in the web for simply supported RC beams, J. Civ. Eng. Constr. Technol. 2 (April (4)) (2011) 82–89. http://www.academicjournals.org/jcect.
[6] A. Ahmed, M.M. Fayyadh, S. Naganathan, K. Nasharuddin, Reinforced concrete beams with web openings: a state of the art review, Mater. Des. 40 (2012) 90–102, doi:http://dx.doi.org/10.1016/j.matdes.2012.03.001.
[7] F.B.A. Beshara, I.G. Shaaban, T.S. Mustafa, Strut-and-Tie modelling of R.C. continuous deep beams, ASEC 2015 Conference in Algeria, 12-15 December 2015 (2015).
[8] J.L. Lafta, K. Ye, Specification of deep beams affect the shear strength cap, Civ. Environ. Res. 8 (2) (2016) 2016. ISSN 2224-5790 (Paper) ISSN 2225-0514 (Online) www.iiste.org.
[9] N. Nair, P.E. Kavitha, Effect of openings in deep beams with varying span to depth ratios using strut and tie model method, IOSR J. Mech. Civ. Eng. (IOSR-JMCE) (2016) 78–81. e-ISSN: 2278-1684,p-ISSN: 2320-334X www.iosrjournals.org.

[10] M. Moradi, R. Esfahani, Application of the strut-and-tie method for steel fiber reinforced concrete deep beams, Constr. Build. Mater. 131 (2017) 423–437, doi:http://dx.doi.org/10.1016/j.conbuildmat.2016.11.042.
[11] L.M. Shather, S.N. Hussein, L.F. Hasan, Theoretical evaluation of RC deep beam with web opening by using nonlinear finite element software [ABAQUS], Int. J. Sci. Eng. Res. 9 (5) (2018) ISSN 2229-5518.
[12] M.A. Mansur, W.A. Alwist, Reinforced fiber concrete deep beams with web opening, Int. J. Cem. Compos. Lightweight Concr. 6 (4) (1984) 263–271.
[13] N.E. Shanmugam, S. Swaddiwudhipong, Strength of fiber reinforced concrete deep beams containing openings, Int. J. Cem. Compos. Lightweight Concr. 10 (1) (1988) 53–60.
[14] A.F. Ashour, Shear capacity of reinforced concrete deep beams, J. Struct. Eng. 126 (September (9)) (2000) 1045–1052.
[15] D.R. Sahoo, C.A. Flores, S.-H. Chao, Behavior of steel fiber-reinforced concrete deep beams with large opening, ACI Struct. J. 109 (2) (2012) 193–204.
[16] J.-H. Doh, T.-M. Yoo, D. Miller, H. Guan, S. Fragomeni, Investigation into the behavior of deep beam with web openings by finite element, Comput. Concr. 10 (6) (2012) 609–630, doi:http://dx.doi.org/10.12989/cac.2012.10.6.609.
[17] B.S. Abduljalil, Shear resistance of reinforced concrete deep beams with opening strengthened by CFRP strips, J. Eng. Dev. 18 (1) (2014) 14–32 ISSN 1813-7822.
[18] M.A. Adam, M. Said, T.M. Elrakib, Shear performance of fiber reinforced self-compacting concrete deep beams, Int. J. Civ. Eng. Technol. (IJCIET) 7 (January-February (1)) (2016) 25–46.
[19] H.K. Hussain, Finite element analysis of deep beam under direct and indirect load, Kufa J. Eng. 9 (2) (2018) 152–167, doi:http://dx.doi.org/10.30572/2018/kje/090212.
[20] C.H. Huang, L.H. Chen, Y.C. Kan, C.H. Wu, T. Yen, Shear Behavior of Full Size Reinforced Lightweight Concrete Beam, Dahan Institute of Technology, Hualien, Taiwan, 2011.
[21] K. Sathiyamoorthy, Shear and Flexural Behaviour of Lightweight Self-Consolidating Concrete Beams, A PhD Thesis Presented to Ryerson University In Partial Fulfillment of the Requirements for the Degree of Master of Applied Science In the Program of Civil Engineering Toronto, Ontario, Canada, 2016.
[22] F. Kong, G. Sharp, Shear strength of lightweight reinforced concrete deep beams with web openings, Struct. Eng. 51 (8) (1973) 267–275.
[23] M. Ramadan, "Experimental Study of Behavior of Reinforced Lightweight Concrete Deep Beams With Web Openings", MSc. Thesis, Ain Shams University, 2017 115pp..
[24] G. Abd Elhameed, "Analytical Study for Behavior of Reinforced Lightweight Concrete Deep Beams With and Without Web Openings", MSc Thesis, Ain Shams University, Egypt, 2018 140 pp..
[25] J.S. Foster, R. Lan Gilbert, Experimental Studies on High- Strength Concrete Deep Beams, ACI Struct. J. 95 (July (4)) (1998) 382–390.
[26] H.M. Alsaeq, Effects of opening shape and location on the structural strength of R.C. Deep beams with openings, World Acad. Sci. Eng. Technol. Int. J. Civ. Environ. Struct. Construct. Architect. Eng. 7 (6) (2013) 494–499.
[27] W.A. Jasim, A. Allawi, N.K. Oukaili, Effect of size and location of square web openings on the entire behavior of reinforced concrete deep beams, Civ. Eng. J. 5 (1) (2019) 209–226.
[28] M.A. Ibrahim, A. El Thakeb, A.A. Mostafa, H.A. Kottb, Experimental study of new reinforcement details for reinforced concrete deep beams with shear opening, Al-Azhar Univ. Civ. Eng. Res. Mag. (CERM) 40 (1) (2018) 347–367.
[29] ANSYS 13.0, Coupled Structural/Thermal Analysis, (ANSYS Tutorials) Copyright 2010 by, University of Alberta, 2010.
[30] E. Montoya, F.J. Vecchio, S.A. Sheikh, Compression field modeling of confined concrete, Struct. Eng. Mech 123 (2001) 231–248.
[31] P. Soroushian, C.D. Lee, 'Constitutive modeling of steel fiber reinforced concrete under direct tension and compression', fiber reinforced cements and concrete: recent developments, Proceedings of International Conference, Cardiff, UK, 1989, pp. 363–377.
[32] P. Marti, Truss models in detailing, Concr. Int. 7 (12) (1985) 66–73.
[33] K.H. Tan, K. Tong, C.Y. Tang, Consistent strut-and-tie model of deep beams with web openings, Mag. Concr. Res. 55 (1) (2003) 65–75.
[34] M.F. Elazab, "Behavior of Reinforced High Strength Concrete Deep Beams With Web Openings", MSc. Thesis, Mansoura University, 2007 169 pp..
[35] ACI Committee 318, Building Code Requirements for Reinforced Concrete and Commentary (ACI 318-14), American Concrete Institute, Farmington, Hills, MI, 2014.
[36] W.E. El-Demerdash, S.E. El-Metwally, M.E. El-Zoughiby, A.A. Ghaleb, Behavior of RC shallow and deep beams with openings via the Strut-and-Tie model method and nonlinear finite element, Arab. J. Sci. Eng. (2015), doi:http://dx.doi.org/10.1007/s13369-015-1678-x ISSN 1319-8025.
[40] European Committee for standardization, EN 1992-1-1 Eurocode-2: Design of Concrete Structures – Part 1-1: General Rules and Rules for Buildings, European Committee, 2004.